Research Article

Propellants, Explosives, Pyrotechnics

doi.org/10.1002/prep.202100372

pep.wiley-vch.de

# Spectroscopic, Structural and Energetic Properties of Pentanitroaniline

**Thomas M. Klapötke,*[a] Burkhard Krumm,*[a] and Christian Riedelsheimer[a]**

*Dedicated to Professor Wolfgang Beck on Occasion of his 90th Birthday.*

**Abstract:** Although pentanitroaniline (PNA) has been known for almost 100 years, as well as with an optimized synthesis, it is still not fully characterized. In this contribution, the crystal structure of PNA is reported for the first time without any adducts or solvents, allowing a view of the crystal packing, as well as the exact positioning of the nitro groups relative to each other. In addition, based on the crystal structure, a Hirshfeld analysis was performed, which determines the distances and types of interactions of the outer atoms. The compound was also studied in detail by NMR, especially with respect to $^{13}C$ and $^{14}N$, making this a challenge due to sensitivity in solution. Furthermore, the compound was fully characterized by IR spectroscopy and TGA, as well as the sensitivities, were measured. Using the density obtained from X-ray crystallography, as well as the heat of formation calculated with the GAUSSIAN program package, the energetic parameters were calculated using EXPLO5 computer code. The performance data were compared to the commonly used RDX and oxidizer ammonium perchlorate, as well as the structurally similar triaminotrinitro (TATB) and pentanitro (PNB) benzene.

**Keywords:** Energetic materials · Hirshfeld Analysis · Polynitrobenzene · NMR spectroscopy · X-ray diffraction

## 1 Introduction

Polynitrobenzenes have been an interesting area of research within energetic materials for well over a century. In this process, some well-known compounds have been created, which are still in use today, among them TNT, styphnic acid and TATB. The benzene-based explosives have the advantage of relatively high decomposition points and high densities. This is especially the case for compounds with hydrogen bonding between amino groups and neighboring nitro groups. In addition, amino-nitro-benzenes often exhibit low sensitivity, which ensures safe handling [1–2].

Pentanitrobenzene (PNB), which was first synthesized by Nielsen *et al.* in 1979 and further fully characterized by us in 2019 including the crystal structure, shows promising performance data with a high density and decomposition temperature [3–4]. The introduction of an amino group at the 'nitro-free' position on the ring could show improved properties due to hydrogen bonding between the amine and the neighboring nitro groups. Already back in 1928 this compound was synthesized and described, as pentanitroaniline (PNA) [5]. Again by Nielsen *et al.*, the synthesis was further improved [6]. However, characterization was mainly based on decomposition point or elemental analysis, and no NMR data or sensitivities were mentioned. In 2006, a crystal structure of PNA was reported as 1,2-dichloro-

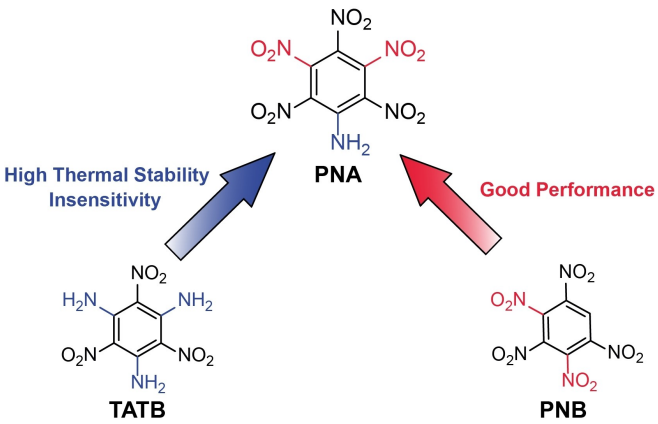


**Figure 1.** Comparison of PNA with TATB and PNB in respect of their advantages.

[a] *T. M. Klapötke, B. Krumm, C. Riedelsheimer*
*Department of Chemistry*
*Ludwig-Maximilian University Munich*
*Butenandtstr. 5–13(D), 81377 Munich, Germany*
*Phone: (+)49 89 2180 77497*
**e-mail: tmk@cup.uni-muenchen.de*
*bkr@cup.uni-muenchen.de*

ethane solvate, followed by the crystal structure as benzene solvate in 2015 [7–8].

In this work, the full characterization and investigation of the properties of pentanitroaniline is performed and compared with the structurally similar TATB and PNB (Figure 1) [9].

## 2 Experimental Section

General: Solvents were dried and purified with standard methods. 3,5-Dinitrobenzoic acid is commercially available and used without further purification. IR spectra were recorded with a Perkin-Elmer Spectrum BX-FTIR spectrometer coupled with a Smiths ATR DuraSample IRII device in the range of 4000–650 $cm^{-1}$ at ambient temperature. NMR spectra were recorded with Bruker TR 400 MHz spectrometers at 25 °C. Chemical shifts were determined in relation to external standards $Me_4Si$ ($^1H$, 399.8 MHz); ($^{13}C$, 100.5 MHz); $MeNO_2$ ($^{14}N$, 28.9 MHz). Elemental analyses (CHN) were obtained with a Vario EL Elemental Analyzer.

The sensitivity data were acquired by measurements with a BAM drophammer and a BAM friction tester. Melting and decomposition points were determined by differential thermal calorimetry (DTA) using an OZM Research DTA 552-Ex instrument at a heating rate of 5 °C $min^{-1}$. Measurements were performed in open glass vessels against a reference material in the range of 25 °C to 400 °C.

The crystal structure data was obtained using an Oxford Xcalibur CCD Diffractometer with a KappaCCD detector at low temperature (122 K). Mo–Kα radiation (λ = 0.71073 Å) was delivered by a Spellman generator (voltage 50 kV, current 40 mA). Data collection and reduction were performed using the CRYSALIS CCD [10] and CRYSALIS RED [11] software, respectively. The structure was solved by SIR92/SIR97 [12] (direct methods) and refined using the SHELX-97 [13–14] software, both implemented in the program package WinGX22 [15]. Finally, the structure was checked using the PLATON software [16]. The images are drawn with thermal ellipsoids at 50% probability level.

The theoretical calculations were achieved by using the Gaussian16 program package [17] and were visualized by using GaussView 6.0.16 [18]. Optimizations and frequency analyses were performed at the B3LYP level of theory (Becke's B3 three-parameter hybrid functional by using the LYP correlation functional) with a cc-pVDZ basis set. After correcting the optimized structures with zero-point vibrational energies, the enthalpies and free energies were calculated on the CBS-4 M (complete basis set) level of theory [19]. The detonation parameters were obtained by using the Explo5 (V6.05.04) program package [20–21].

**CAUTION**! Pentanitroaniline (**2**) is an energetic material and shows sensitivities in the range of secondary explosives! Manipulation with caution during synthesis or manipulation and additional protective equipment (leather jacket, face shield, ear protection, Kevlar gloves) is strongly recommended.

### 3,5-Dinitroaniline (1)

3.5-Dinitrobenzoic acid (2.03 g, 9.57 mmol) was added to a mixture of conc. sulfuric acid (2.5 mL), oleum (20%, 8 mL) and chloroform (10 mL) at room temperature. The mixture was heated to 35 °C, and sodium azide (0.70 g, 10.8 mmol) was added. The solution was refluxed for 5 h and afterward cooled back to room temperature and poured onto ice water. After filtration and washing with ice-cold water, **1** was obtained as a yellow-brown solid (1.26 g, 72%).

**$^1$H NMR** ([$D_6$]DMSO): δ = 7.89 (t, $^4J_{H,H}$ = 2.1 Hz, 1H, C*H*), 7.73 (d, 2H, C*H*), 6.5 (br, 2H, N$H_2$) ppm. **$^{13}$C NMR** ([$D_6$]DMSO): δ = 151.2 (*C*N$H_2$), 148.8 (*C*N$O_2$), 112.4 (*C*H), 103.7 (*C*H) ppm. **$^{14}$N NMR** ([$D_6$]DMSO): δ = −13 (*NO*$_2$) ppm. **Elemental Analysis**: $C_6H_5N_3O_4$ (183.12): calc. C 39.35, H 2.75, N 22.95%; found C 39.56, H 2.49, N 22.72%.

### Pentanitroaniline (2)

3,5-Dinitroaniline (**1**, 0.91 g, 4.93 mmol) was dissolved in conc. $H_2SO_4$ (15.5 mL) and oleum (20%, 9 mL). The solution was cooled by an ice bath and nitric acid (1.7 mL) was added dropwise. Afterward, the solution was heated to 72–75 °C for 90 min and then stirred for further 1 h back at 0 °C. A yellow precipitate was formed, which was filtered using a glass frit. The wet precipitate was re-dissolved in 1,2-dichloroethane and the solution was decanted to separate the aqueous acidic phase of the remaining sulfuric acid. The solution was stored in a −32 °C freezer overnight, and **2** was obtained as bright-yellow crystalline solid (0.52 g, 33%) after filtration.

**$^1$H NMR** ([$D_6$]acetone): δ = 8.6 (br, 2H, N*H*) ppm. **$^{13}$C NMR** ([$D_6$]acetone): δ = 143.3 (*C*1-N$H_2$), 142.9/131.1 (*C*2/*C*3/*C*5/*C*6), 124.2 (*C*4) ppm. **$^{14}$N NMR** ([$D_6$]acetone): δ = −27/−30/−31 (*NO*$_2$) ppm. **Elemental Analysis**: $C_6H_2N_6O_{10}$ (318.11): calc. C 22.65, H 0.63, N 26.42%; found C 22.74, H 0.88, N 26.24%. **IR (ATR)**: $\tilde{\nu}$ = 3476 (w), 3461 (m), 3373 (m), 3354 (m), 3232 (w), 3097 (vw), 3068 (vw), 2907 (w), 2875 (w), 2646 (w), 1629 (m), 1608 (m), 1581 (s), 1564 (vs), 1542 (vs), 1534 (vs), 1463 (m), 1442 (m), 1421 (s), 1362 (m), 1349 (m), 1327 (s), 1285 (vs), 1285 (vs), 1171 (m), 1046 (m), 967 (w), 914 (m), 889 (vs), 852 (w), 830 (s), 803 (m), 786 (m), 762 (w), 753 (w), 741 (w), 726 (w), 674 (m), 650 (m), 620 (s), 591 (m), 583 (m), 543 (m), 491 (s) $cm^{-1}$. **DTA** (5 °C $min^{-1}$): 190 °C (dec.). **Sensitivities (BAM)**: impact 2 J, friction 80 N (grain size 100–500 μm).

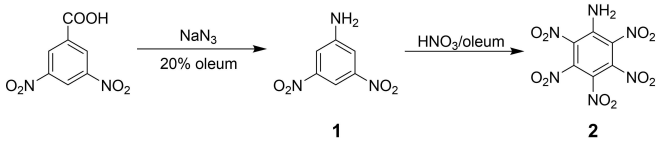


**Scheme 1.** Synthesis of PNA (**2**) starting from 3,5-dinitrobenzoic acid.

## 3 Results and Discussion

### 3.1 Synthesis

In a first step, 3,5-dinitroaniline is prepared from 3,5-dinitrobenzoic acid by a *Schmidt* reaction, converting the carboxyl group into amine via *in situ* generation of $HN_3$. Oleum is used to dissolve the 3,5-dinitrobenzoic acid and also to eliminate any water formed during the reaction (Scheme 1). After refluxing, the reaction mixture is quenched on ice and the aniline **1** is obtained as a solid in good yield and purity [8].

Again **1** is dissolved in oleum and conc. nitric acid is added under cooling. While the solution is heated, PNA (**2**) already precipitates as a golden-yellow precipitate. Without quenching, the precipitate is filtered and then re-dissolved in 1,2-dichloroethane. This allows the remaining traces of sulfuric acid to be removed, and after storing the solution overnight at −32 °C, PNA (**2**) crystallizes as bright-yellow plates [8].

### 3.2 NMR Spectroscopy

3,5-Dinitroaniline (**1**) and pentanitroaniline (**2**) were characterized by $^{1}H$, $^{13}C$, and $^{14}N$ NMR spectroscopy in [$D_6$]DMSO for **1** and [$D_6$]acetone for **2**.

The $^{1}H$ NMR spectrum of **1** shows a triplet at 7.89 ppm, which can be assigned to the ring hydrogen at C4, a doublet at 7.73 ppm for the other two aromatic hydrogens at C2 and C5 as well as a broadened resonance at 6.5 ppm for the amino group. The $^{13}C$ NMR spectrum shows the four expected signals at 151.2, 148.8, 112.4, and 103.7 ppm; and the $NO_2$ resonance is detected at −13 ppm in the $^{14}N$ NMR spectrum.

[$D_6$]Acetone is the only solvent in which PNA (**2**) is sufficiently soluble in order to detect resonances. Immediate measurements after solution were required, however, also fast decomposition signals occur.

In the $^{1}H$ NMR spectrum, PNA (**2**) shows only one broadened resonance at 8.6 ppm, which can be assigned to the amino group. In the $^{13}C$ NMR spectrum of a concentrated sample, the expected four resonances were visible after a short acquisition time. Due to the attached nitro groups, the carbon resonances are significantly broadened and require concentrated solutions in addition to a longer acquisition time. Only the carbon atom next to the amino group (C1) shows no broadening at 143.3 ppm. Apart from C4, which is detected at 124.2 ppm, an exact assignment of C2 and C3 at 142.9 ppm and 131.1 ppm is not possible. However, after a few minutes already, signals of decomposition products can be detected at 143.3 ppm and 143.2 ppm, which increase with time. For the $^{14}N$ NMR spectrum, the same effect was observed. At the beginning of the measurement three resonances for the nitro groups were detected at −27, −30, and −31 ppm. After a few minutes, new signals were observed at −23 and −25 ppm, which also increase with time and correspond to decomposition products. Very likely, these are products of hydrolysis, formed by nucleophilic substitution of nitro by hydroxyl groups, similar as observed for pentanitrobenzene [4].

### 3.3 Single Crystal Structure Analysis

Suitable single crystals for X-ray structure determination of **2** were obtained from dichloromethane by slow evaporation at ambient temperature. PNA crystallizes as orange plates in the tetragonal space group $P\bar{4}2_1c$ with a density of 1.926 g cm$^{-3}$ at 122 K (Table 1). The structure with selected bond lengths and angles is shown in Figure 2.

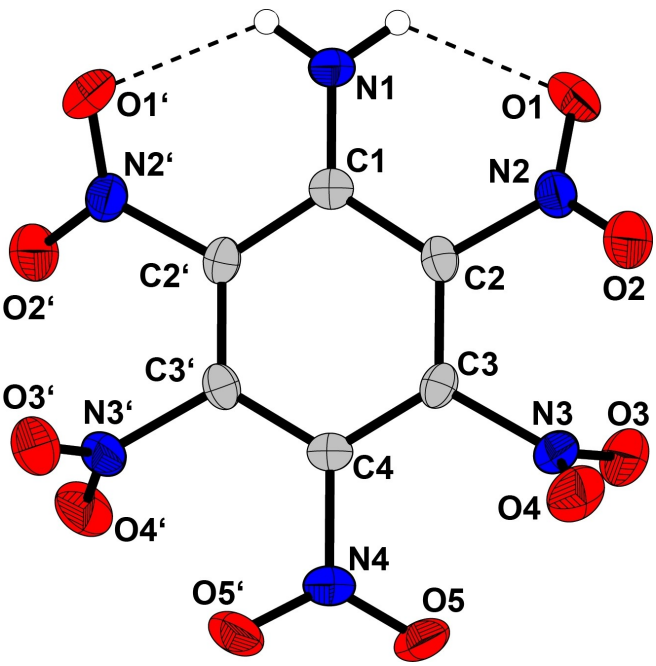


**Figure 2.** X-ray molecular structure of **2**. Selected distances [Å] and angles [°]: C1–C2 1.428(5), C2–C3 1.377(5), C3–C4 1.391(5), N4–C4 1.458(7), N3–C3 1.481(5), N2–C2 1.465(5), N1–C1 1.319(7), O2–N2 1.221(4), O1–H 2.082(4) C2–C3–C4 121.4(4), C1–C2–N2 118.5(4), N1–C1–C2 122.9(2), C2′–C1–C2–C3 1.0(2), C4–C3–C2–C1 −2.1(5), N1–C1–C2–C3 −179.0(2), N1–C1–C2–N2 3.8(4), N3–C3–C4–N4 0.8(4), O1–N2–C2–C1 −34.0(5), O3–N3–C3–C4 −75.0(4), O5–N4–C4–C3 −29.8(2).

**Table 1.** Crystal data, details of the structure determinations and refinement of **2**.

| | PNA |
|---|---|
| formula | $C_6H_2N_6O_{10}$ |
| *FW* [g mol$^{-1}$] | 318.11 |
| *T* [K] | 122 |
| λ [Å] | 0.71073 |
| crystal system | tetragonal |
| space group | $P\bar{4}2_1c$ |
| crystal size [mm] | 0.09×0.36×0.43 |
| crystal habit | orange plate |
| *a* [Å] | 8.7959(3) |
| *b* [Å] | 8.7959(3) |
| *c* [Å] | 28.3660(16) |
| $\alpha$ [deg] | 90 |
| $\beta$ [deg] | 90 |
| $\gamma$ [deg] | 90 |
| *V* [Å$^3$] | 2194.62(16) |
| *Z* | 8 |
| $\rho_{calc.}$ [g cm$^{-3}$] | 1.926 |
| $\mu$ [mm$^{-1}$] | 0.19 |
| F(000) | 1280 |
| 2Θ range [deg] | 1.436 −26.370 |
| index ranges | $-10 \le h \le 10$<br>$-10 \le k \le 10$<br>$-35 \le l \le 35$ |
| reflections collected | 32085 |
| reflections unique | 28543 |
| parameters | 212 |
| GooF | 1.0730 |
| $R_1/wR_2$ [I > 2σ(I)] | 0.0440/0.0882 |
| $R_1/wR_2$ (all data) | 0.0688/0.0976 |
| max/min residual electron density [Å$^{-3}$] | −0.220/0.220 |
| CCDC | 2118338 |

There is symmetry along the C1–C4 plane, resulting in equal bond lengths and angles on both sides. The benzene ring shows almost complete planarity and only the nitro groups twist out of the plane. However, the benzene ring shows different C–C bond lengths. The C1–C2 bond (1.428 Å) is significantly longer compared to the C2–C3 (1.377 Å) and C3–C4 (1.391 Å) bonds, similar as also observed for 2,3,4,6-tetranitroaniline (C1–C2 1.429 Å, C2–C3 1.379 Å, C3–C4 1.383 Å) [4]. This can be explained by the electron pushing amine group, which pushes electrons into the bond, and as a consequence the bond length is shortened. Comparing the bond lengths with benzene derivatives with uniform groups, such as hexaaminobenzene and hexanitrobenzene, equal bond lengths of about 1.39 Å are observed [22–23]. The same effect is seen with the different C–N bond lengths. Thus, the length of the C1–N1 bond (1.319 Å) is also shorter than that of the other C–$NO_2$ bonds (1.458–1.481 Å).

Considering the different nitro groups, especially the $NO_2$ groups in *meta* position are more twisted relative to the benzene ring (torsion angle −75.0°). The nitro groups in *ortho* and *para* position are less twisted with a torsion angle of −34.0° (*ortho*) and −29.8° (*para*). The slightly stronger twisting of the *ortho* $NO_2$ groups compared to the *para* group can be explained by the hydrogen bonds of the *ortho* oxygens with the hydrogen atoms of the amine group (O1···H 2.082 Å).

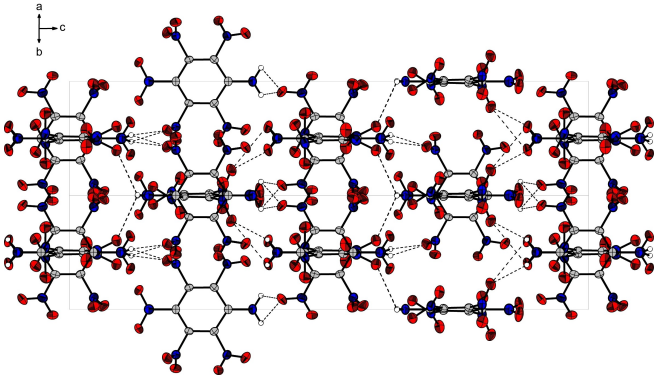


**Figure 3.** View of the unit cell of PNA (**2**) with hydrogen bonds between the hydrogen atoms and oxygen atoms along the axis between *a* and *b* axes.

The unit cell of PNA is shown along the *a* and *b* axes in Figure 3, displaying the alternation of the molecules with an angle of 90° to each other. This increases the intermolecular distance between the nitro groups and results in less repulsive interactions. In addition, the intermolecular hydrogen bonds between the hydrogen atoms of the amine group and oxygen atoms of neighboring molecules are illustrated. The alternating twisting of the molecules and nitro groups can thus shorten the distance from the oxygen atoms to the hydrogens, allowing the formation of attractive hydrogen bonds with bond lengths between 2.3 Å and 2.7 Å.

### 3.4 Thermal Stabilities and Energetic Properties

The physical and energetic properties of PNA were determined and summarized in Table 2 and further compared to the common secondary RDX, oxidizer ammonium perchlorate (AP), and the structurally similar TATB and PNB.

The thermal stability of **2** was determined by Differential Thermal Analysis (DTA) measurement with a heating rate of 5 °C min$^{-1}$ in the temperature range of 15–400 °C. PNA does not melt before decomposing at 190 °C (onset temperature) and shows the lowest decomposition temperature of all compared compounds. The same trend can be observed for the sensitivities (IS = 2 J, FS = 80 N, ESD = 200 mJ). In terms of impact and friction sensitivity, the values of PNA and PNB are almost in the same range, except for ESD for which PNB is more sensitive with a value of 63 mJ.

Comparing the different densities of the compounds, it is notable that PNA and PNB have the same density (1.88 g cm$^{-3}$), and TATB has a slightly higher density, which can be explained by the higher number of hydrogen bonds.

**Table 2.** Physical and energetic properties of PNA (**2**) compared to RDX, TATB, PNB and AP.

| | PNA (2) | RDX | TATB | PNB | AP |
|---|---|---|---|---|---|
| Formula | $C_6H_2N_6O_{10}$ | $C_3H_6N_6O_6$ | $C_6H_6N_6O_6$ | $C_6HN_5O_{10}$ | $NH_4ClO_4$ |
| *FW* [g mol$^{-1}$] | 318.11 | 222.12 | 258.15 | 303.10 | 117.49 |
| $T_{melt}$ [°C][a] | – | 200 | – | 143 | – |
| $T_{dec}$ [°C][a] | 190 | 208 | ca. 350 | 220 | 240 |
| *IS* [J][b] | 2 | 8 | >25 | 5 | 20 |
| *FS* [N][b] | 80 | 120 | >355 | 96 | 360 |
| *ESD* [mJ][c] | 200 | 250 | 293 | 63 | >726 |
| $\rho$ [g cm$^{-3}$][d] | 1.88 | 1.79 | 1.93 | 1.88 | 1.95 |
| *O* [%][e] | 50.3 | 43.22 | 37.19 | 52.8 | 54.5 |
| $\Omega_{CO}$ [%][f] | 15.1 | 0 | −18.6 | 18.5 | 34.0 |
| $\Omega_{CO2}$ [%][f] | −15.1 | −21.61 | −55.8 | −13.2 | 34.0 |
| $\Delta_f H_m°$ [kJ mol$^{-1}$][g] | 39.6 | 70.3 | −154.2 | 66.4 | −295.8 |
| EXPLO5 V6.05.04 | | | | | |
| $V_{det}$ [m s$^{-1}$][h] | 8808 | 8801 | 8201 | 8932 | 6855 |
| $p_{det}$ [GPa][h] | 34.9 | 33.6 | 28.0 | 36.9 | 18.0 |
| $I_{sp}$ [s][i] | 251 | 263 | 188 | 250 | 154 |
| $I_{sp}$ [s] (15 % Al)[i] | 263 | 274 | 219 | 260 | 234 |
| $I_{sp}$ [s] (15 % Al, 14 % binder)[i] | 236 | 241 | 209 | 246 | 257 |

[a] Onset melting $T_{melt}$ and decomposition point $T_{dec}$ from DTA measurements, heating rate 5 °C min$^{-1}$. [b] Sensitivity towards impact *IS* and friction *FS*. [c] Electrostatic discharge sensitivity (OZM ESD tester). [d] RT densities are recalculated from X-ray densities, if not otherwise noted. [e] Oxygen content. [f] Oxygen balance assuming formation of CO or $CO_2$. [g] Heat of formation calculated at CBS-4 M level using GAUSSIAN09 [19]. [h] Predicted detonation velocity and detonation pressure. [i] Specific impulse $I_{sp}$ of the neat compound and compositions with aluminum or aluminum and binder (6 % polybutadiene acrylic acid, 6 % polybutadiene acrylonitrile and 2 % bisphenol A ether) using EXPLO5 (Version 6.05.04) program package (7 MPa, isobaric combustion, equilibrium to throat and frozen to exit.) [20].

PNA exhibits a positive oxygen balance assuming the formation of CO and an oxygen content slightly above 50 %. Thus, the values are in the same range as PNB and far above those of TATB and RDX.

The various energetic properties were calculated by using the EXPLO5 (V6.05.04) software. As a result, PNA has a detonation velocity almost identical to RDX (PNA: 8808 m s$^{-1}$, RDX: 8801 m s$^{-1}$) and only PNB has a slightly higher value of 8932 m s$^{-1}$, whereas TATB and especially AP have lower values (TATB: 8201 m s$^{-1}$, AP: 6855 m s$^{-1}$). The same trend can be observed for the detonation pressure, as well as specific impulse. However, this does not apply to the specific impulse with aluminum and binder, since ammonium perchlorate has the highest value (257 m s$^{-1}$), closely followed by PNB (246 m s$^{-1}$) and PNA (236 m s$^{-1}$).

### 3.5 Hirshfeld Analysis

With the crystal structure of PNA, further in-depth analysis and comparison with structurally similar compounds TATB and PNB can be performed. Thereby, the compounds differ only slightly by different functional groups, which in turn lead to different interactions and thus have a direct influence on the sensitivities. For this reason, Hirshfeld surfaces were created based on the crystal structures of the compounds (Figure 4) [4, 24–25].

The 2D fingerprint plots show the distance and the types of interaction of atoms to surrounded atoms in the crystal packing. The plots are given as a function of $d_i + d_e$, whereby $d_i$ is the distance from the Hirshfeld surface to the nearest atom interior and $d_e$ is the distance from the Hirshfeld surface to the nearest atom exterior [26]. Based on the different types, amounts and strengths of the interactions, a conclusion can be expressed regarding the different sensitivities of structurally similar compounds [25].

Equiatomic interactions exhibit a destabilizing effect, which increases the sensitivity. The size of the atoms has a decisive impact, which is the reason that O···O interactions have a higher influence than N···N or H···H interactions [27–28]. The same is observed for the O···N, C···O and C···N interactions. However, these have less influence compared to the equiatomic interactions. If there are strong destabilizing interactions at certain positions, these are indicated as red dots in the Hirshfeld plots. From this it can be concluded that with a higher number of such red dots there is an increased sensitivity [27, 29].

Stabilizing interactions are mainly intermolecular hydrogen bonds, which in turn reduce the sensitivity. These bonds prevent the displacement of individual layers by external influences. Thus, hydrogen bonds are the interactions that are mainly observed in insensitive compounds [30].

Apart from the different types of interactions, the relative strengths of the interactions are also important for the

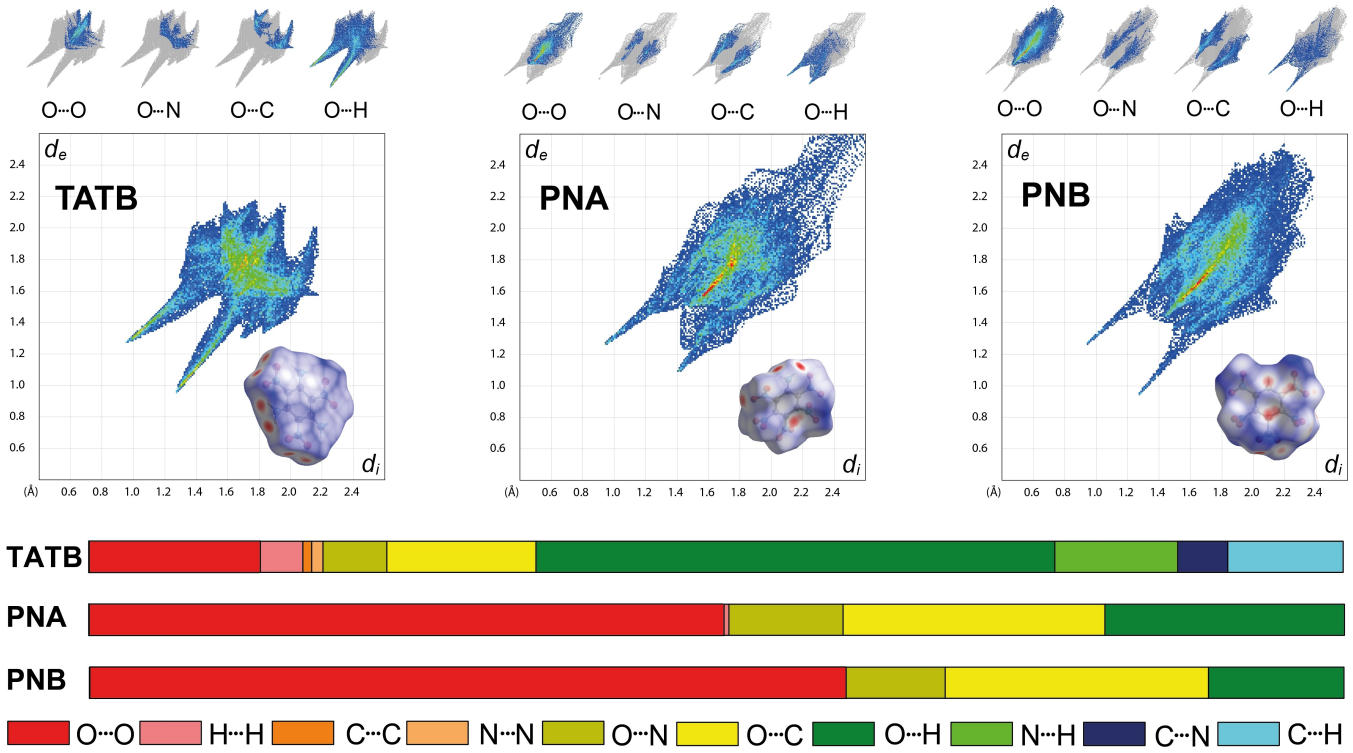


**Figure 4.** On top, the 2D fingerprint plot of the crystal stacking and the corresponding Hirshfeld surface of TATB, PNA (**2**) and PNB. The population of close contacts are shown below.

sensitivities. These can be extracted and determined from the position in the 2D fingerprint plot [25].

As expected, in the case of TATB the strongest stabilizing interactions are between oxygen and hydrogen (O···H). In addition to these hydrogen bonds, N···H interactions are also found extensively in TATB. PNA also features hydrogen bonding, but in a much smaller amount, and even PNB exhibits O···H interactions that, unlike TATB or PNA, take place with the hydrogen-bonded to the benzene ring. When looking at the destabilizing O···O bonds, the exact opposite trend is seen. TATB shows by far the least amount of such interactions (14%), whereas PNB has the most (60%), closely followed by PNA (51%). In addition to the destabilizing O···O interactions, all compounds also exhibit slightly destabilizing O···C interactions. Again, TATB shows the lowest number of 12%, whereas PNB and PNA show the same number of 21%. The high total number of destabilizing interactions compared to stabilizing ones in PNA and PNB is also reflected in the experimentally measured sensitivities. Thus, the direct comparison of TATB and PNA shows that the two additional amino groups form so many additional hydrogen bonds that the sensitivity is so much lower. In the direct comparison of PNB to PNA, both compounds show similarly measured sensitivities and that although PNA has a larger number of hydrogen bonds and a lower number of O···O interactions. A possible reason for this could be the stronger interactions of the oxygens, which are in a region of $d_e + d_i = 3.2$ Å for PNA and $d_e + d_i = 3.4$ Å for PNB. In addition, the O···H interactions of PNA are also slightly weaker than those of PNB.

## 4 Conclusion

After almost 100 years, pentanitroaniline is now fully characterized and can be prepared via a two-step synthesis starting from easily available 3,5-dinitrobenzoic acid. The crystal structure of PNA was obtained for the first time without any solvent or adducts by low-temperature X-ray crystallography. NMR data were finally obtained, especially with respect to $^{13}C$ and $^{14}N$. The $^{13}C$ NMR spectrum showed the expected broadened resonances, because of the neighboring nitro groups, as well as three distinguishable resonances in the $^{14}N$ NMR spectrum. However, because of the moisture sensitivity issues of PNA, the NMR measurements had to be performed in [$D_6$]acetone, in which decomposition of the PNA was observed already after a few minutes. Nevertheless, it was possible to identify the resonances of PNA. Based on the crystal structure a Hirshfeld analysis was performed and compared to the similar TATB and PNB. Furthermore, important physical and chemical properties were determined and discussed, such as sensitivities, thermal stability and energetic parameters. These properties are quite in the range of RDX or even better in

some cases. Unfortunately, PNA shows similar to PNB, a high moisture sensitivity, which restricts further chemistry and applications.

## *Acknowledgements*

For financial support of this work by Ludwig-Maximilian University (LMU), the Office of Naval Research (ONR) under grant no. ONR N00014-19-1-2078 and the Strategic Environmental Research and Development Program (SERDP) under contract no. W912HQ19C0033 are gratefully acknowledged. Open access funding enabled and organized by Projekt DEAL.

## References

[1] C. D. Hutchinson, V. K. Mohan, R. W. Millar, Aminotetryls: Synthesis, Spectral Characterization, Thermal Decomposition and Explosive Properties, *Propellants, Explos. Pyrotech.* **1984**, *9*, 161–171.

[2] V. M. Boddu, D. S. Viswanath, T. K. Ghosh, R. Damavarapu, 2,4,6-Triamino-1,3,5-trinitrobenzene (TATB) and TATB-based Formulations–A Review, *J. Hazard. Mat.* **2010**, *181*, 1–8.

[3] A. T. Nielsen, R. L. Atkins, W. P. Norris, Oxidation of Poly(nitro)anilines to Poly(nitro)benzenes. Synthesis of Hexanitrobenzene and Pentanitrobenzene, *J. Org. Chem.* **1979**, *44*, 1181–1182.

[4] T. Huber, C. v. d. Heide, T. M. Klapötke, B. Krumm, Synthesis, Characterization, and Properties of Pentanitrobenzene $C_6H(NO_2)_5$, *Z. Anorg. Allg. Chem.* **2019**, *645*, 126–132.

[5] B. Flürscheim, E. L. Holmes, Pentanitroaniline, *J. Chem. Soc.* **1928**, 3041–3046.

[6] R. L. Atkins, A. T. Nielsen, C. Bergens, Synthesis of Polynitrobenzenes. Oxidation of Polynitroanilines and Their *N*-Hydroxy, *N*-Methoxy, and *N*-Acetyl Derivatives, *J. Org. Chem.* **1984**, *49*, 503–507.

[7] S. V. Rosokha, J. J. Lu, S. M. Dibrov, J. K. Kochi, 2,3,4,5,6-Pentanitroaniline 1,2-Dichloroethane Disolvate: 'Push-Pull' Deformation of Aromatic Rings by Intramolecular Charge Transfer, *Acta Crystallogr.* **2006**, *C62*, o464–o466.

[8] A. Preimesser, Ph. D. Thesis, *Energetic Materials Based on Benzenes, 2,2'-Bisimidazole and 1,2,4,5-Tetrazines*, Ludwig-Maximilians-Universität Munich, Germany, **2015**.

[9] T. M. Klapötke, *Energetic Materials Encyclopedia*, 2nd Edition, De Gruyter, Berlin/Boston, **2021**.

[10] CRYSALIS CCD, 1.171.35.11 ed., Oxford Diffraction Ltd., Abingdon, Oxford (U. K.), **2011**.

[11] CRYSALIS RED, 1.171.35.11 ed., Oxford Diffraction Ltd., Abingdon, Oxford (U. K.), **2011**.

[12] A. Altomare, M. C. Burla, M. Camalli, G. L. Cascarano, C. Giacovazzo, A. Guagliardi, A. G. G. Moliterni, G. Polidori, R. Spagna, SIR97: A New Tool for Crystal Structure Determination and Refinement, *J. Appl. Crystallogr.* **1999**, *32*, 155–119.

[13] G. M. Sheldrick, *Programs for Crystal Structure Determination*, University of Göttingen, Germany, **1997**.

[14] G. M. Sheldrick, A Short History of SHELX, *Acta Crystallogr.* **2008**, *64 A*, 112–122.

[15] L. Farrugia, WinGX Suite for Small-molecule Single-crystal Crystallography, *J. Appl. Crystallogr.* **1999**, *32*, 837–838.

[16] A. L. Spek, Structure Validation in Chemical Crystallography, *Acta Crystallogr.* **2009**, *65D*, 148–155.

[17] M. J. Frisch, G. W. Trucks, H. B. Schlegel, G. E. Scuseria, M. A. Robb, J. R. Cheeseman, G. Scalmani, V. Barone, B. Mennucci, G. A. Petersson, H. Nakatsuji, M. Caricato, X. Li, H. P. Hratchian, A. F. Izmaylov, J. Bloino, G. Zheng, J. L. Sonnenberg, M. Hada, M. Ehara, K. Toyota, R. Fukuda, J. Hasegawa, M. Ishida, T. Nakajima, Y. Honda, O. Kitao, H. Nakai, T. Vreven, J. A. Montgomery Jr., J. E. Peralta, F. Ogliaro, M. J. Bearpark, J. Heyd, E. N. Brothers, K. N. Kudin, V. N. Staroverov, R. Kobayashi, J. Normand, K. Raghavachari, A. P. Rendell, J. C. Burant, S. S. Iyengar, J. Tomasi, M. Cossi, N. Rega, N. J. Millam, M. Klene, J. E. Knox, J. B. Cross, V. Bakken, C. Adamo, J. Jaramillo, R. Gomperts, R. E. Stratmann, O. Yazyev, A. J. Austin, R. Cammi, C. Pomelli, J. W. Ochterski, R. L. Martin, K. Morokuma, V. G. Zakrzewski, G. A. Voth, P. Salvador, J. J. Dannenberg, S. Dapprich, A. D. Daniels, Ö. Farkas, J. B. Foresman, J. V. Ortiz, J. Cioslowski, D. J. Fox, Gaussian, Inc., Wallingford, **2009**.

[18] R. D. Dennington, T. A. Keith, J. M. Millam, *GaussView*, Ver. 6.0.16 ed., Semichem Inc., Shawnee Mission, KS, **2016**.

[19] J. A. Montgomery, M. J. Frisch, J. W. Ochterski, G. A. Petersson, A Complete Basis Set Model Chemistry. VII. Use of the Minimum Population Localization Method, *J. Chem. Phys.* **2000**, *112*, 6532–6542.

[20] M. Sućeska, *EXPLO5 V.6.05*, Zagreb, **2020**.

[21] M. Sućeska, Calculation of the Detonation Properties of C–H–N–O Explosives, *Propellants, Explos. Pyrotech.* **1991**, *16*, 197–202.

[22] D. A. Dixon, J. C. Calabrese, J. S. Miller, The Structure of Hexaaminobenzene, *Angew. Chem. Int. Ed.* **1989**, *28*, 90–92.

[23] Z A. Akopyan, Y. T. Struchkov, V. G. Dashevii, Crystal and Molecular Structure of Hexanitrobenzene, *J. Struct. Chem.* **1966**, *7*, 385–392.

[24] H. H. Cady, A. C. Larson, The Crystal Structure of 1,3,5-Triamino-2,4,6-trinitrobenzene, *Acta Crystallogr.* **1965**, *18*, 485–496.

[25] Y. Ma, A. Zhang, C. Zhang, D. Jiang, Y. Zhu, C. Zhang, Crystal Packing of Low-Sensitivity and High-Energy Explosives, *Cryst. Growth Des.* **2014**, *14*, 4703–4713.

[26] J. J. McKinnon, M. A. Spackman, A. S. Mitchell, Novel Tools for Visualizing and Exploring Intermolecular Interactions in Molecular Crystals, Acta Crystallogr., *Sect. B: Struct. Sci.* **2004**, *60*, 627–668.

[27] C. Zhang, X. Xue, Y. Cao, Y. Zhou, H. Li, Intermolecular Friction Symbol Derived from Crystal Information, *CrystEngComm* **2013**, *15*, 6837–6844.

[28] M. Reichel, D. Dosch, T. M. Klapötke, K. Karaghiosoff, Correlation between Structure and Energetic Properties of Three Nitroaromatic Compounds: Bis(2,4-dinitrophenyl) Ether, Bis(2,4,6-trinitrophenyl) Ether, and Bis(2,4,6-trinitrophenyl) Thioether, *J. Am. Chem. Soc.* **2019**, *141*, 19911–19916.

[29] D. E. Dosch, M. Reichel, M. Born, T. M. Klapötke, K. Karaghiosoff, Investigation of Structure–Property Relationships of Three Nitroaromatic Compounds: 1-Fluoro-2,4,6-trinitrobenzene, 2,4,6-Trinitrophenyl Methanesulfonate, and 2,4,6-Trinitrobenzaldehyde, *Cryst. Growth Des.* **2021**, *21*, 243–248.

[30] M. A. Spackman, J. J. McKinnon, Fingerprinting Intermolecular Interactions in Molecular Crystals, *CrystEngComm.* **2002**, *4*, 378–392.

Manuscript received: December 22, 2021
Revised manuscript received: February 3, 2022
Version of record online: March 25, 2022